Heliyon 10 (2024) e28256

Contents lists available at ScienceDirect

Heliyon

journal homepage: www.cell.com/heliyon

Research article

Biomimetic nanocarriers loaded with temozolomide by cloaking brain-targeting peptides for targeting drug delivery system to promote anticancer effects in glioblastoma cells

Huaming Chen [a,1], Yunhong Wang [a,1], Hai Wang [a], Kun Zhang [b], Yunfei Liu [c], Qiangfeng Li [a], Chengli Li [a], Zhonghui Wen [a,**], Ziyu Chen [d,*]

[a] Department of Neurosurgery, Pu'er People's Hospital, Pu'er, 665099, China
[b] Department of Emergency, Pu'er People's Hospital, Pu'er, 665099, China
[c] Department of Ultrasound Medicine, Pu'er People's Hospital, Pu'er, 665099, China
[d] Department of Nephrology, Pu'er People's Hospital, Pu'er, 665099, China

ARTICLE INFO

Keywords:
Apoptosis
Blood-brain barrier
Glioblastoma
Temozolomide
Zein

ABSTRACT

Glioma is the leading cancer of the central nervous system (CNS). The efficacy of glioma treatment is significantly hindered by the presence of the blood-brain barrier (BBB) and blood-brain tumour barrier (BBTB), which prevent most drugs from entering the brain and tumours. Hence, we established a novel drug delivery nanosystem of brain tumour-targeting that could self-assemble the method using an amphiphilic Zein protein isolated from corn. Zein's amphiphilicity prompted it to self-assembled into NPs, efficiently containing TMZ. This allowed us to investigate temozolomide (TMZ) for glioblastoma (GBM) treatment. To construct TMZ-encapsulated NPs (TMZ@RVG-Zein NPs), the NPs' Zein was clocked to rabies virus glycoprotein 29 (RVG29). To verify that the NPs could penetrate the BBB and precisely target and kill the GBM cancer cell line, in vitro studies were performed. The process of NPs penetrating cancer cell membranes was investigated using enzyme-linked immunosorbent assays (ELISAs) to measure the expressions of nicotinic acetylcholine receptors (nAChRs) on the U87 cell line. Therefore, effective targeted brain cancer treatment is possible by forming NP clocks, a cell-penetrating natural Zein protein with an RVG29. These NPs can penetrate the blood-brain barrier (BBB) and enter the glioblastoma (U87) cell line to release TMZ. These NPs have a distinct cocktail of biocompatibility and brain-targeting abilities, making them ideal for involving brain diseases.

1. Introduction

Glioblastoma (GBM) multiforme is the underlying cause of about half of all new malignant tumours in the CNS. Chemotherapy and radiation are the gold standards for treating GBM when surgical resection is not an option [1]. There is an immediate need for novel techniques and enhanced technologies to address the limited and poor therapeutic options for GBM. Nanotechnology's ability to strengthen pharmacological systemic administration and absorption has offered great therapeutic alternatives for various ailments

* Corresponding author. No. 44 Zhenxing Avenue, Simao District, Pu'er, 665099, Yunnan, China.
** Corresponding author. No. 44 Zhenxing Avenue, Simao District, Pu'er, 665099, Yunnan, China.
E-mail addresses: Zhonghuiwen190@outlook.com (Z. Wen), Ziyu_Chen84@outlook.com (Z. Chen).
[1] Contribute equally to this study.

https://doi.org/10.1016/j.heliyon.2024.e28256
Received 25 January 2024; Received in revised form 13 March 2024; Accepted 14 March 2024
Available online 15 March 2024

during the past few decades [2]. The complex pathways involved in GBM's initiation, progression, and invasion raise concerns that a monotherapy approach may cause cancer cells to develop tolerance to the drug, which in turn could cause metastasis and recurrence. This suggests that these problems should be amenable to therapy with a combination of drugs having diverse action mechanisms [3–5]. Current treatments have several significant flaws, such as a short half-life in circulation, poor delivery to sick areas, and problems managing the release of several drugs at the right spots. These problems hinder effective tumour removal by preventing therapeutic drugs from accumulating in tumour cells. Furthermore, the tumour's location makes the BBB an essential and substantial obstacle to drug administration. No small-molecule drug or large-molecule pharmaceutical can cross the BBB. Extended blood circulation, sufficient transportation across the blood-brain barrier, efficient internalization, and controlled drug release within GBM cells are all challenges to the drug administration of GBM therapy [6]. All these steps are necessary to ensure sufficient therapeutic agent accumulation in GBM cells. Treatments for glioblastoma have used nanotechnology to enhance therapeutic efficacy by avoiding these physiological restrictions [7]. Despite several in vitro and in vivo studies demonstrating the effectiveness and therapeutic potential of nanocarriers and nanotechnology, there has been a shortage of published clinical trials for GBM nano-therapies. Glioma patients have also benefited from thermotherapy, phototherapy, immunotherapy, and gene therapy as an adjunct to standard treatment [8].

Zein is a plant-based protein with many benefits, such as biocompatible, abundant, high drug binding capacity, and minimal cytotoxicity. To accomplish the stability and specificity of Zein-based DDSs, a range of ligand changes can be made to take advantage of Zein's unique protein structure. Anticancer drugs encapsulated in Zein-based DDSs reach the bloodstream after injection or oral delivery [9]. Incorporating PEG or cancer cell membrane into the DDS, which has a lengthy circulation half-life, makes evading immune cell clearance possible [10]. A higher concentration of anticancer drugs in tumour tissue can be achieved by conjugating Zein-based DDSs with targeting polypeptides or tumour microenvironment response chemicals, hence obtaining the targeting capacity [11]. Accurate cancer treatment will then be possible. Zein-based DDSs have a lengthy residence duration for oral delivery within the gastrointestinal tract because they shield unstable anticancer drugs from degradation by enzymes or highly acidic conditions [12–14].

The two most common phrases used to describe drugs on a surface level are (i) intracellular drug delivery and (ii) extracellular drug delivery. The second option has piqued medical researchers' interest since it offers a potent means of bringing about specific biological effects by introducing biomolecules into the cytosol or another intracellular compartment [15–17]. Passage through the lipid bilayer was the primary obstacle for quite some time. Since micelles could carry various compounds, including hydrophobic drugs, proteins, and even genes, they offered a long-awaited solution to this transportation problem. Over time, transportation networks grew more complex, and now we can take pride in having a variety of methods that allow for the practical delivery of drugs to specific locations [18]. The impact resolution will enable us to easily classify these techniques as macro, micro, or nano. Direct cell penetration and enhanced permeability are two methods that rely on membrane disruption to allow substances to enter the plasma membrane; other methods include endocytic pathways, *trans*-membrane transporter proteins, and membrane fusion [19–21]. Over the past ten years, numerous cutting-edge methods have been developed that make it possible for tiny peptide shuttles, brain-permeable peptide-drug conjugates (PDCs), and cell-penetrating peptides (CPPs) to penetrate the brain's parenchyma and endothelial cells. Encapsulating our target pharmaceuticals within biocompatible carriers that enhance their plasma life and stability is crucial for achieving a delayed-release pattern [22]. The upshot is that peptide-based drug delivery technologies outperform conventional pharmaceuticals. CPPs are one example of a method for intracellular drug delivery. In addition, peptides are preferred for targeted drug administration since most physiological ligands in circulation are proteins, peptides, or peptide-conjugated complexes [23].

The 29-amino acid sequence found in the Rabies virus glycoprotein (RVG29) allows it to attach to nicotinic acetylcholine receptors competitively. RVG29 can cross the blood-brain barrier (BBB) and enter the brain via nicotinic acetylcholine receptors, allowing it to carry genes, nucleic acids, and drugs. RVG29 is a promising peptide for administering drugs for treating several disorders, including Parkinson's disease and cancers of the brain, including gliomas [24–26]. One possible therapeutic use of RVG29 is the delivery of siRNA to mitigate the chronic consequences of TBI. Recent research has shown that RVG29 can target neuronal mitochondria with solid-lipid nanoparticles coated with macrophage membranes [27]. In sporadic Alzheimer's disease, neuronal mitochondria malfunction is caused by increased reactive oxygen species. Potentially utilized to halt the advancement of Alzheimer's disease, RVG29 transports functional antioxidants into the brain. This provides more evidence that peptides can be effective BBB modes of delivery [28,29].

Currently, the first-line chemotherapy for glioblastoma is temozolomide (TMZ). The percentage of patients claimed to be alive at two years has reportedly grown from 10.4% to 26.5%, and the median overall survival has been raised to 14.6 months, according to TMZ [30–32]. One of the rare drugs that can reach the brain's parenchyma and have a therapeutic impact is TMZ. Since TMZ's fundamental issue is its poor stability, only a portion of the administered amount can cross the BBB. The inert 5-aminoimidazole-4--carboxamide (AIC) and the methylating agent are the byproducts of the product's quick degradation [33]. Methylation at the O6 guanine site, brought about by MTIC, is thought to be the primary source of TMZ chemotherapeutic toxicity. This prodrug has a half-life that is significantly affected by pH, lasting less than 2 h in physiological settings (pH = 7.4) and around 24 h in an acidic environment (pH $<$ 4 at 25 °C). This means that the blood-borne degradation of systemically administered TMZ could prevent its active metabolite, MTIC, from penetrating the BBB [34]. The therapeutic efficacy is diminished when TMZ hydrolysis products are formed before reaching the central nervous system. The patient is exposed to significant side effects such as hematological toxicity, acute cardiomyopathy, oral ulceration, hepatotoxicity, and pneumocystis pneumonia due to the short half-life of TMZ, which requires numerous high doses [35]. To enhance its concentration in the brain while minimizing the potential of adverse systemic effects, TMZ could be reformulated utilizing carriers to provide more effective BBB. Alternatively, it could be administered through multiple routes [31].

To treat GBM, this study aimed to engineered TMZ@RVG-Zein NPs, which are Zein-based NPs encapsulated with RVG29 (Fig. 1). This is the first report we know of that addresses the delivery of TMZ for targeted GBM therapy by RVG29 clocking with a cell-

penetrating protein (Zein). Zein, a naturally occurring protein, is being utilized as a drug carrier for the first time to treat central nervous system diseases in vivo.

2. Experimental section

2.1. Materials

Temozolomide (TMZ) was acquired from Dalian MeiLun Biotechnology Co., Ltd. RVG29-Cys peptide (sequence: N term-YTIWMPENPRPGTPCDIFTNSRGKRASNGC-Cys) was synthesized by American Peptide Company (Sunnyvale, CA, USA). Phenazine methosulfate (PMS), dimethyl sulfoxide, Zein, coumarin-6 (C6), and paraformaldehyde (PFA) were acquired from Hongquan Biotechnology Co., Ltd. All remaining reagents, if not specified, were purchased from Shanghai Titan Science Co. (Shanghai, China). Live/Dead cell imaging kits, STYO 9, and propidium iodide (PI) were purchased from Thermo Fisher Scientific (Waltham, MA, USA). ELISA kits were bought from Shanghai Yuanxin Biotechnology Co., Ltd. Fetal bovine serum (FBS), Phosphate buffered saline, Dulbecco's modified Eagle's medium (DMEM), Tyrisin and L-glutamine were provided by Gibco. Cleaved caspase-3 and Caspase-3 antibodies were bought from Dojindo Laboratories (Kumamoto, Japan). Annexin V-FITC/PI apoptosis detection kit and D-luciferin were supplied by Shanghai Yeasen Corporation. All other chemicals were available from commercial sources and used without further purification.

2.2. Cell culture

Human glioblastoma U87 cells were purchased from the Chinese Academy of Sciences (Shanghai, China). U87 cell lines were cultured in 10% FBS, 1% L-glutamine, 1% penicillin, and 1% streptomycin-contained DMEM mediums. A mouse brain capillary endothelial cells (bEnd.3) were cultured in DMEM containing 10% FBS, L-glutamine, 1% penicillin, and 1% streptomycin. The incubation was conducted under a 5% CO_2 atmosphere, 95% relative humidity, and 37 °C.

3. Characterization of NPs

Scanning electron microscopy (SEM) images were measured on microscopy (Sigma 300, ZEISS/Sigma 300) under an acceleration voltage of 3 kV. Fourier evaluated the chemical bond structure transform infrared spectroscopy (FTIR; Thermo Scientific Nicolet iN10, USA). Dynamic Light Scattering (DLS, ALv/CGS-3, German) and Zeta potential analyzer (Brookhaven Instruments Corporation, NanoBrook Omni, USA) were employed to analyze the physical properties. The optical density (OD) was measured by a microplate reader (Molecular Devices, SpectraMaxM5, USA). Cell morphology was observed by confocal laser scanning microscopy (CLSM, LSM 510 Metanlo, Zeiss Co., Germany). Immunofluorescence staining was observed using a fluorescence microscope (Olympus, IX83, Japan). Statistical calculations were performed using GraphPad Prism (V.8.0.2).

3.1. Formation of the nanoencapsulation of TMZ

TMZ@Zein NPs were developed by encapsulating TMZ through the self-assembly of Zein [11]. In brief, an aqueous ethanol solution containing Zein and TMZ in a mass ratio 7:1 was prepared. A nitrogen evaporator evaporated the solvent, and TMZ@Zein NPs were the byproduct. A membrane dialysis bag removed the excess TMZ with a molecular (3 kD-MWCO). Next, the TMZ@Zein NPs that had been purified were stored at −4 °C.

RVG29 and TMZ@Zein conjugation to develop TMZ@RVG-Zein.

Fig. 1 shows the reaction phases for the TMZ@Zein NPs coupling with the RVG29 peptide. To develop the mixture, we first suspended TMZ@Zein NPs in ethanol and then added PBS until the pH reached 7.5; the last PBS concentration was 45%. A cross-linker sulfo-SMCC was immersed in the mixture in a 10:1 M ratio with Zein. A maleimide-activated form of Zein NPs, SMCC-TMZ@Zein NPs, was fabricated by reacting the surface Zein molecules of TMZ@Zein NPs with sulfo-SMCC. The Zein's amino group (NH_2) was activated

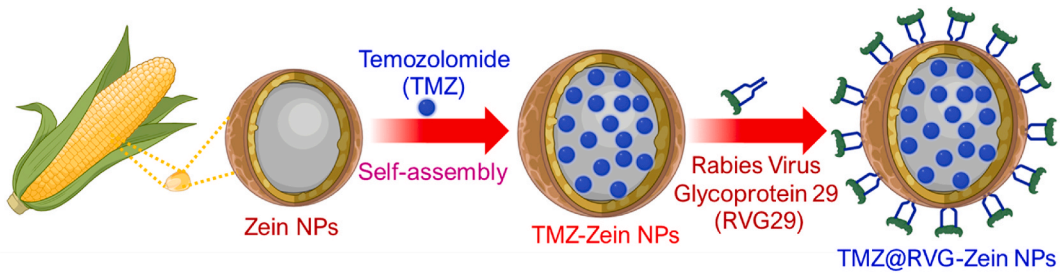

Fig. 1. Scheme of the formation of TMZ@RVG-Zein NPs. Design of the TMZ@RVG-Zein NPs. Zein's amphiphilicity prompted it to self-assemble into NPs, efficiently containing TMZ. This allowed us to investigate temozolomide (TMZ) for glioblastoma (GBM) treatment. To TMZ-encapsulated NPs (TMZ@RVG-Zein NPs), the NPs' Zein was clocked to rabies virus glycoprotein 29 (RVG29).

by reacting it with sulfo-SMCC. The SMCC-TMZ@Zein NPs were refined by removing any surplus of sulfo-SMCC with the help of a dialysis bag membrane (MWCO-3 kD). In PBS (pH = 7.4), SMCC-TMZ@Zein NPs and RVG29-Cys were combined in a 1.1:1 M ratio. The maleimide groups of SMCC-TMZ@Zein NPs were coupled with the RVG29-Cys thiol groups to fabricate TMZ@RVG-Zein NPs. Any additional RVG29-Cys was eliminated using a dialysis bag membrane. We were using the previous research to determine RVG29-Cys's conjugation efficiency.

3.2. Loading efficiency (LE) and encapsulation efficiency (EE)

After the formation of TMZ@RVG-Zein NPs, the supernatant was collected by centrifugation (10000 rpm, 5 min). The amount of TMZ in the supernatant was determined via UV spectroscopy according to the standard curve [36]. The following equation calculated the encapsulation efficiency of TMZ@RVG-Zein NPs:

Encapsulation efficiency (%) = (total amount of feeding drug-number of drugs in supernatant)/total amount of feeding drug × 100%.

3.3. TMZ release of TMZ@RVG-Zein NPs

The drug release profile of TMZ from TMZ@RVG-Zein NPs was examined in various buffer solutions of pH = 7.4 without and with 10% serum. TMZ@RVG-Zein NPs were dispersed in 1 mL of the corresponding buffer solution to the 2 mg/mL concentration, and then the solutions were sealed in a dialysis bag with MWCO of 3kD. The dialysis bags were immersed in 10 mL buffer solutions of pH = 7.4 with or without 10% serum and placed in a shaker at 37 °C. Within a specified time, 1 mL sample solution was removed from the buffer solution, and an equivalent amount of fresh buffer solution was added. Meanwhile, the concentration of TMZ in the solutions at different time points was determined by UV–vis.

3.4. MTT and LIVE/DEAD assay

The in vitro cytotoxicity assay was performed with the MTT assay. U87 cell lines were seeded under the down chamber of 24-well (1×10^5 cell line per well) and cultured in DMEM medium (0.5 mL per well) containing 10% FBS, 10 mM glucose, and 10 mM lactate for 24 h. Afterwards, TMZ, RVG-Zein NPs, and TMZ@RVG-Zein NPs were placed in the up chamber of the assay with various concentrations and co-incubated for 24 h. To determine cytotoxicity, MTT solution (10 μL) was mixed in each well, and the plate was incubated for another 4 h. Then, the MTT contained culture medium was replaced with DMSO (100 μL). Absorbance values of formazan were measured with a microplate reader (Bio-Rad model-680) at 490 nm (corrected for background absorbance at 630 nm) [37].

The anticancer efficacy was further considered over the LIVE/DEAD assay. After different treatments, the cell culture medium was removed. Then, a fresh medium containing calcein-AM (5 μg/mL) and PI (10 μg/mL) was mixed. After 25 min, the cells were rinsed with PBS and imaged by a fluorescence microscope.

3.5. The cell membranes' nAChR expression

To investigate the precise targeting method, ELISA was used to evaluate the level of the nAChRs expression on the surface of the U87 and bEnd.3 cells. The antibody that targets nAChR was then placed on an ELISA microplate. We assessed the protein doses and used the micro-ELISA plate to determine the expression of nAChR at the same protein concentration. The nAChR concentration was measured by recording the fluorescence density at 450 nm. The nAChR expression values were examined by the previous procedure [38].

3.6. Cellular uptake

To cellular uptake investigation of the TMZ, TMZ@RVG-Zein NPs, and TMZ@Zein NPs stained with coumarin-6 (C6) into U87 cell line, and the cells were seeded on six-well microplates with the density of 3×10^5 cells per well and cultured overnight. After that, cells were cultured in a medium containing Cy5/TMZ, TMZ@RVG-Zein NPs, and TMZ@Zein (TMZ equivalent concentration of 0.1 μg/mL) for 1 h duration. After the treatment, cells were washed with PBS, digested by trypsin, and then collected for analysis using fluorescent inverted microscopy to evaluate the cellular uptake behaviour of U87 cells incubated with different samples [39].

To cellular uptake investigation of the TMZ, TMZ@RVG-Zein NPs, and TMZ@Zein NPs stained with coumarin-6 (C6) by flow cytometry. For comparison, cells were incubated with Cy5/TMZ@Zein NPs, Cy5/TMZ@RVG-Zein NPs, and Cy5/TMZ, respectively, for 4 h. After the final incubation, cells were washed using PBS and then collected for quantitative analysis. After the final incubation, cells were rinsed using PBS and collected for flow cytometry analysis [40,41,41].

3.7. Cell proliferation assay

CLSM measured the cell proliferation of U87 cells. Briefly, U87 cells were planted in a 12-well plate at a density of 3×10^5 cells per well with 1.0 mL medium and treated with TMZ@RVG-Zein NPs (0, 0.1, and 0.2 μM) incubated for 6 h. After incubation, the cells were stained by DAPI, Rabbit antihuman Caspase-3 antibody, for immunofluorescence assay. After the cells were washed with PBS three

times, the secondary antibody of goat anti-rabbit IgG H&L was added. Finally, the culture medium was removed, and the cells were washed with PBS three times. CLSM performed the immunofluorescence images.

3.8. Apoptosis analysis by flow cytometry

A flow cytometer measured the apoptosis of U87 cells. Briefly, U87 cells were planted in a 12-well plate at a density of 1×10^5 cells per well with 1.0 mL medium and incubated for 24 h. Then, the cells were treated with TMZ, TMZ@RVG-Zein NPs, and TMZ@Zein NPs for 2 h. After that, the culture medium was removed, and the cells were washed with PBS three times [42].

3.9. In vitro permeability assay

For cell permeabilization assay, bEnd.3 cells were seeded into the upper chamber of the transwell insert and incubated for 24 h. Seven days of culture, the confluence of the cells at 80% and the monolayer cell mimicked the BBB/BBTB activity and morphology. The medium in the upper chamber was replaced with 100 μL of serum-free medium containing Cy5/TMZ, Cy5/TMZ@Zein NPs, and Cy5/

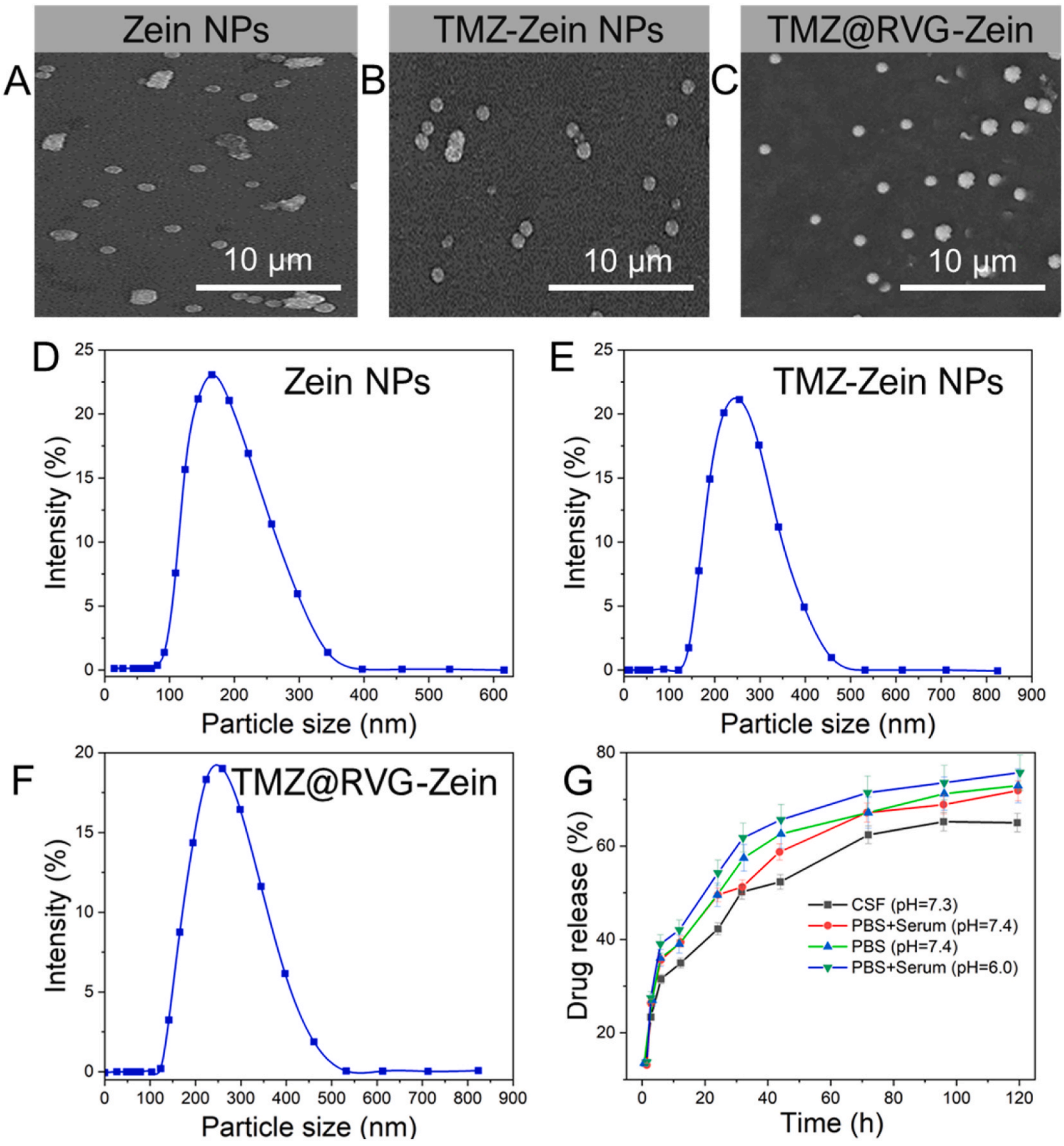

Fig. 2. The morphological characterizations and stability examinations of Zein NPs, TMZ@Zein NPs, and TMZ@RVG-Zein NPs. A-C) Scanning electron microscope (SEM) images of Zein NPs, TMZ@Zein NPs, and TMZ@RVG-Zein NPs. Scale bar = 10 μm. D-F) The NPs size of Zein NPs, TMZ@Zein NPs, and TMZ@RVG-Zein NPs. G) TMZ release from TMZ@RVG-Zein NPs in the PBS (pH = 7.4), CSF (pH = 7.3), PBS with 10% serum (pH = 6.0), and PBS with serum (pH = 7.4). Data were stated as means ± SEM (n = 3).

TMZ@RVG-Zein NPs. A migration inducer medium (600 μL) was placed in the lower chamber. After incubation for 4 h, cells in the upper compartment were removed, and those on the lower surface of the membrane were the migrated cells. After a culture of 4 h, the culture medium of the upper chamber was eliminated and rinsed. IVIS Imaging verified the fluorescence of the basolateral and apical chambers.

3.10. Statistical analysis

All data presented are from at least three independent experiments, and the experimental data are expressed as mean ± standard deviation. For comparisons, the two-tailed Student's t-test was performed. Statistically significant difference was set at *p < 0.05, **p < 0.01, ***p < 0.001, ****p < 0.0001. The statistical analysis was performed using GraphPad Prism 8 software.

4. Results and discussion

4.1. Fabrication and characterization of Zein nanoparticles

Fig. 2A–C shows the scanning electron microscopy (SEM) analyses of TMZ@Zein NPs and TMZ@RVG-Zein NPs, illustrating their shape and size distribution. The TMZ@Zein NPs and the TMZ@RVG-Zein NPs showed uniformly sized, well-dispersed spherical particles. Dynamic light scattering (DLS) examined the Zein NPs, RVG-Zein NP, and TMZ@RVG-Zein NPs' sizes, surface charges, and polydispersity index (PDI) in the dispersions. The average hydrodynamic dimensions of Zein NPs, RVG-Zein NPs, and TMZ@RVG-Zein NPs were 186.54 ± 2.5, 203.48 ± 1.94, and 220.54 ± 2.5 nm, respectively, as shown in Fig. 2D–F. After TMZ was enclosed, TMZ@Zein NPs were somewhat more significant (18.45 nm) than Zein NPs. Both TMZ@RVG-Zein NPs and TMZ@Zein NPs were 14.42 nm bigger after RVG29 conjugation. According to the results, the PDI values for Zein NPs, RVG-Zein NPs, and TMZ@RVG-Zein NPs were 0.069 ± 0.02, 0.067 ± 0.03, and 0.049 ± 0.02, respectively. These values show A distribution of NPs, all of which are less than 0.1. The values of the zeta-potentials for Zein NPs, RVG-Zein NPs, and TMZ@RVG-Zein NPs were −17.58 ± 0.97, −19.57 ± 1.59, and −11.48 ± 1.27 mV, respectively.

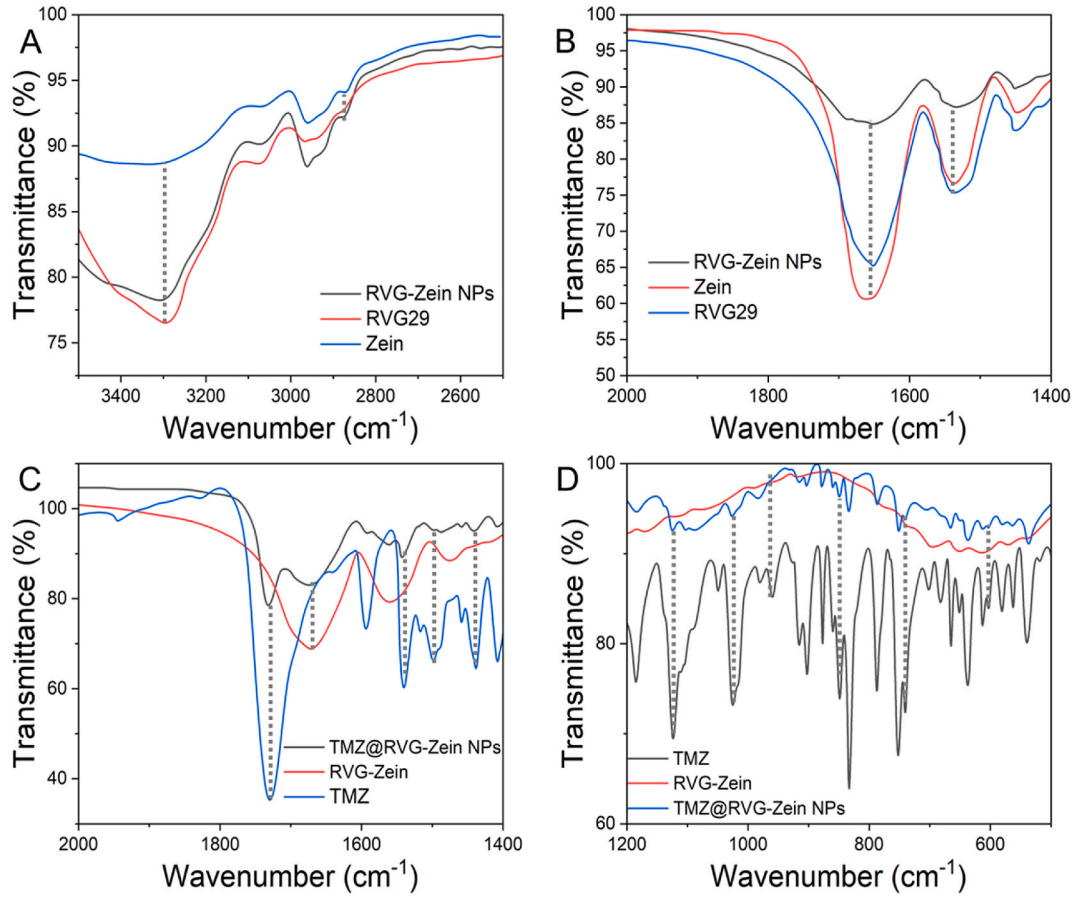

Fig. 3. The structural characterizations Zein NPs, RVG29, TMZ@Zein NPs, and TMZ@RVG-Zein NPs. A and B) Fourier transform infrared (FTIR) spectra of Zein NPs, RVG29, and RVG-Zein NPs. C and D) FTIR spectral analysis of TMZ, RVG-Zein NPs, and TMZ@RVG-Zein NPs.

The TMZ@RVG-Zein NPs had an encapsulation efficiency (EE) of 77.9 ± 4.7% and a loading efficiency (LE) of 66.7 ± 2.9 mg/g. The RVG29-clocking Zein protein (RVG-Zein) is an effective drug carrier, and the great EE and LE showed that the TMZ was encapsulated effectively. Zein and RVG were successfully fabricated with a 96.98 ± 0.17% conjugation efficiency.

FTIR analysis confirmed the RVG clocking Zein conjugation and the RVG-Zein integrated with TMZ. The –OH group vibration stretching at 3290 and the amide A′ group peak found at 2935 cm^{-1} were identified as Zein's fingerprints in Fig. 3A. Amide I's C–N stretching and Amide II's C═O stretching contributed to fingerprints at 1655 and 1545 cm^{-1}, respectively. Due to the large quantities of related chemical bonds in RVG29, the fingerprints at 3291, 1652, and 1545 cm^{-1} were significantly more intense in RVG29 than Zein, even though both are amino acids. The spectra of RVG-Zein showed the same peaks with similar intensities, suggesting that the RVG and Zein were successfully conjugated. The spectra of RVG-Zein and Zein showed a band at 1415 cm^{-1}, which is glutamine, but RVG29 did not, supporting the result that glutamine of Zein and RVG. Fig. 3B further strengthens this finding, which shows that RVG29 does not contain glutamine.

The fingerprints of TMZ were displayed at 1720 cm^{-1}, 1572 cm^{-1}, 1514 cm^{-1}, and 1408 cm^{-1}, respectively, in Fig. 3C and D. These wavelengths were recognized as the C–N bonding and the carbonyl group (C═O), and it was found that the patterns of the TMZ were evident in the spectra of TMZ@RVG-Zein NPs but did not appear in the spectra of RVG-Zein. The results showed that RVG-Zein effectively encapsulated TMZ to achieve TMZ@RVG-Zein nanoparticles.

4.2. TMZ release and stability investigations

The TMZ from TMZ@RVG-Zein NPs was studied in vitro at 37 °C utilizing various conditions, including simulated cerebrospinal fluid (CSF) with a pH = 7.3, pH = 7.4 of PBS, pH = 6.0 of PBS with 10% serum by volume, and pH = 6.0 of PBS with 10% serum by volume (Fig. 2G). Within 24 h, the amount released was 36.99 ± 2.8% in cerebrospinal fluid (CSF), 54.89 ± 3.9% in pH = 7.4 PBS with serum, 50.87 ± 4.7% in pH = 7.4 PBS without serum, and 60.78 ± 3.2% in pH = 6.0 PBS with serum. CSF had a very slow-release rate compared to the other options. At 100 h, the total amount of TMZ@RVG-Zein NPs released was 57.2 ± 2.7% in CSF (pH = 7.3), 75.3 ± 1.8% in PBS (pH = 7.4) with serum, 72.7 ± 3.4% in PBS (pH = 7.4) without serum, and 82.9 ± 3.8 % in PBS (pH = 6.0) with serum, respectively.

The stability of TMZ@RVG-Zein NPs was investigated by dissolving the TMZ@RVG-Zein in a PBS solution containing 10% serum. The solution was then stored at 4 °C for 4 h and 37 °C for 4 h. The measured particle size change during 72 h. The size of TMZ@RVG-Zein NPs grew from 220.54 ± 2.5 to 230.21 ± 3.1 nm at 4 °C and from 220.54 ± 2.5 to 239.40 ± 4.2 nm at 37 °C. The fact that the

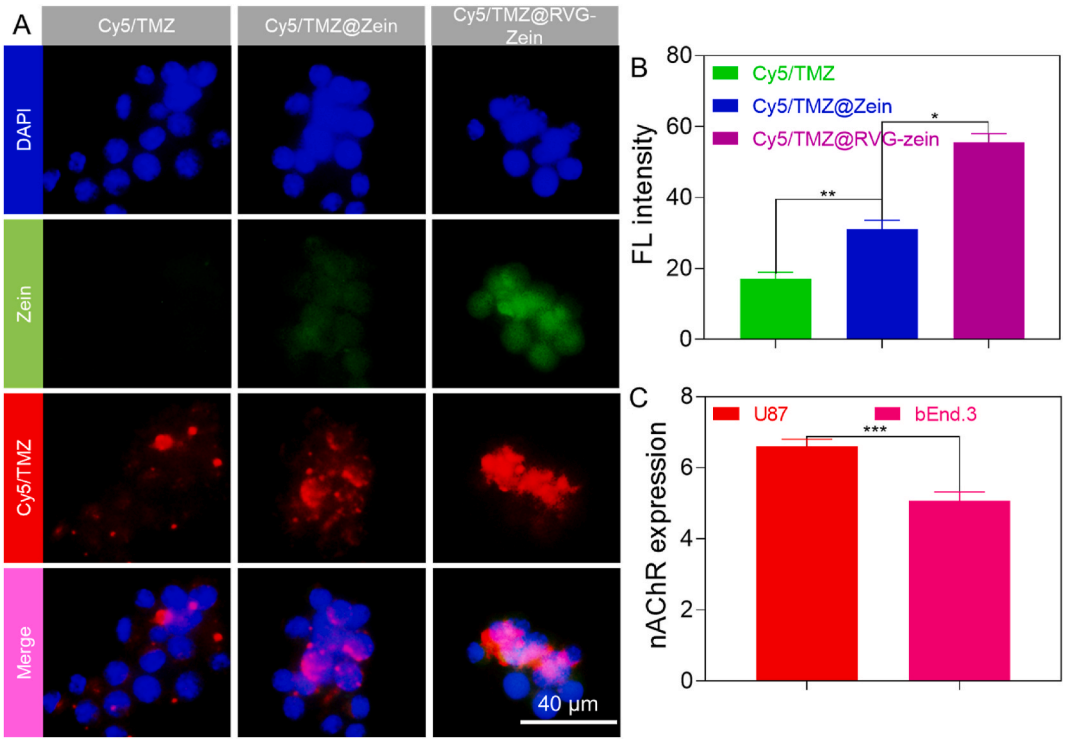

Fig. 4. The cellular uptake of TMZ, TMZ@Zein NPs, and TMZ@RVG-Zein NPs. A) The U87 cells treated with Cy5/TMZ, Cy5/TMZ@Zein and Cy5/TMZ@RVG-Zein NPs for 1 h. The scale bar is 40 μm. The fluorescence intensities of Cy5/TMZ, Cy5/TMZ@Zein and Cy5/TMZ@RVG-Zein NPs for 1 h. C) The expression level of nAChR in bEnd.3 and U87 cells. Data were stated as means ± SEM (n = 3). *P < 0.05, **P < 0.01, ***P < 0.001, compared with control group.

TMZ@RVG-Zein NPs exhibited no size change in the serum solution indicates their excellent stability.

4.3. In vitro cellular uptake

Fig. 4 shows the results of a confocal laser scanning microscopy (CLSM) investigation into the cellular uptake of TMZ@RVG-Zein and TMZ@Zein in U87 cells. After Cy5/TMZ was formed by clocking Cy5 with the drug TMZ, it was encapsulated to develop Cy5/TMZ@Zein and Cy5/TMZ@RVG-Zein NPs. The Zein surface of the Cy5/TMZ@RVG-Zein and Cy5/TMZ@Zein compounds were coupled with a coumarin-6 (C6, fluorescent dye), respectively. After 1 h of treatment with Cy5/TMZ, the U87 cell lines were subjected to Cy5/TMZ@RVG-Zein and Cy5/TMZ@Zein tagged with C6, respectively. Fig. 4A shows that the cytoplasm of the U87 cell line exhibited green fluorescence provided by C6 and red fluorescence produced by Cy5/TMZ, respectively, 1 h intervals of Cy5/TMZ, Cy5/TMZ@Zein, and Cy5/TMZ@RVG-Zein. Quickly penetrating cell lines were both Cy5/TMZ@Zein and Cy5/TMZ@RVG-Zein. Fig. 4A shows that the red fluorescence was uniformly dispersed throughout the cytoplasm and had a distinct boundary. These findings demonstrated that the Cy5/TMZ@Zein and Cy5/TMZ@RVG-Zein molecules could penetrate the cell line. The measured fluorescence intensities displayed in Fig. 4B. The significant expressions of nAChR on the U87 cell line membrane (Fig. 4C) demonstrated that Zein aided cell membrane penetration, while RVG29 increased cellular uptake via endocytosis. After 1 h, the intensity of red fluorescence of Cy5/TMZ@RVG-Zein was noticeably higher than that of Cy5/TMZ@Zein. This suggests that the clocking of RVG onto the NP's surface enhanced the U87 cellular uptake more than Zein alone. Based on the CLSM results, it was determined that Cy5/TMZ@Zein and Cy5/TMZ@RVG-Zein could penetrate the U87 cell line. Potentially helpful in delivering anticancer drugs with poor solubility and bioavailability, Zein and RVG29 enhanced the NPs' cellular absorption.

The outcome was further validated by the flow cytometry-based investigation of cellular uptake. Fig. 5A and B displayed the gating method. When TMZ was labeled with Cy5, the resulting compound was Cy5/TMZ. Similarly, TMZ@RVG-Zein and TMZ@Zein were labeled with Cy5 to produce Cy5/TMZ@RVG-Zein and Cy5/TMZ@Zein, respectively. Treatment of the U87 cell line with Cy5/TMZ@Zein, Cy5/TMZ@RVG-Zein, and Cy5/TMZ for 4 h resulted in cellular uptake of 77.38% for Cy5/TMZ@RVG-Zein and 54.73% for Cy5/TMZ@Zein. The results show that RVG and Zein helped with NP uptake by cell line. However, RVG29 was more effective than Zein NPs (Fig. 5C–F). We believe this is because the NP cellular uptake is enhanced by the receptor-mediated endocytosis linked with RVG29, compared to the Zein-mediated penetration of the cell membrane. Fig. 6A–H shows the results of an investigation into NP cellular uptake mechanisms using various endocytosis inhibitors. Before adding the inhibitors, the U87 cell line was pre-incubated with Cy5/TMZ, Cy5/TMZ@Zein, and Cy5/TMZ@RVG-Zein. At 4 °C, NP uptake by the U87 cell line was significantly reduced compared to 37 °C, indicating that energy-dependent endocytosis, and not energy-independent processes, appropriately regulated cellular uptake of the TMZ@RVG-Zein. The levels of cellular absorption of the NPs were not significantly different between the control group and the group that received nystatin plus cytochalasin D. It showed that caveolae-mediated endocytosis and macropinocytosis

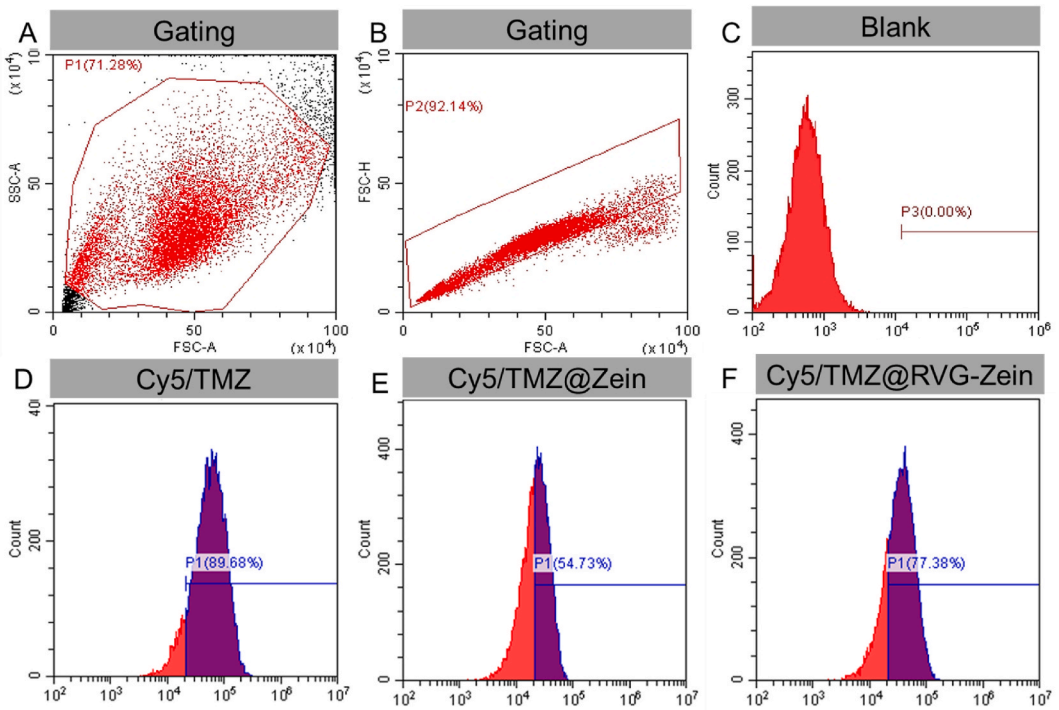

Fig. 5. Cellular uptake by the gating strategy of flow cytometry. A-B) To investigate the percentage of the TMZ and Cy5/TMZ, Cy5/TMZ@Zein and Cy5/TMZ@RVG-Zein NPs in Fig. 5C–F.

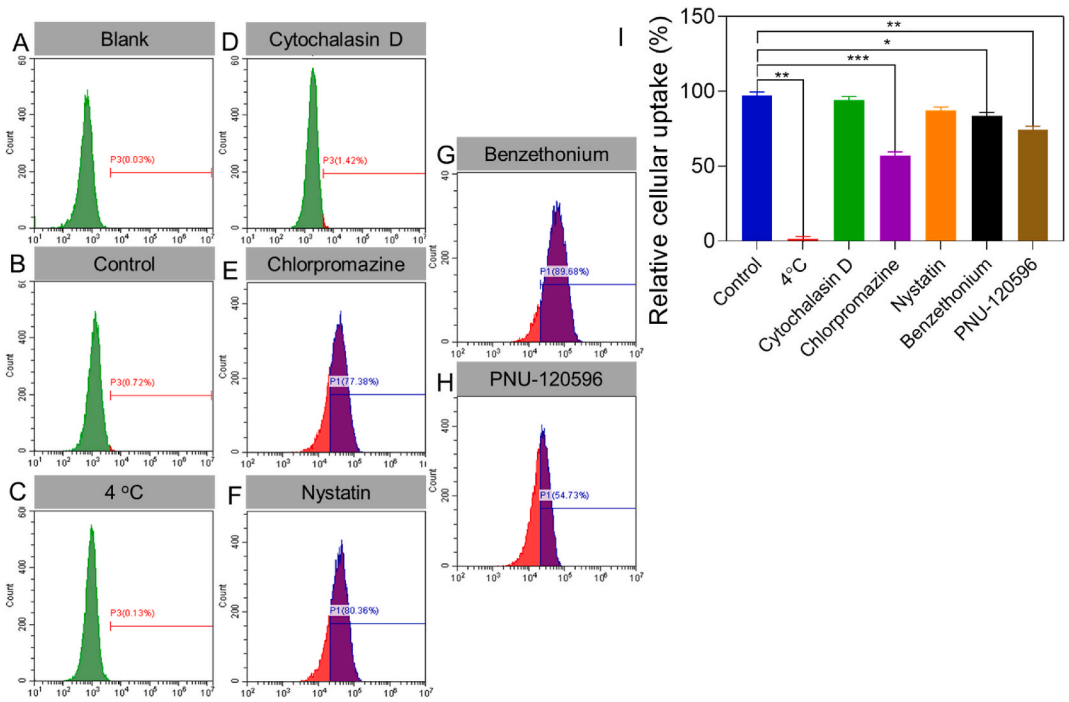

Fig. 6. Representative plots for the cellular uptake of Cy5/TMZ@RVG-Zein NPs by U87 cells after 2 h incubation at 37 °C measured using flow cytometry. A-F) Incubation at 4 °C was applied to prevent energy-dependent endocytosis. Cytochalasin D is the inhibitor of macropinocytosis. Chlorpromazine is the inhibitor of clathrin-mediated endocytosis. Nystatin is the inhibitor of caveolae/lipid raft-mediated endocytosis. G-H) Benzethonium chloride and PNU-120596 are the inhibitors of nAChR-mediated endocytosis. I) Statistical outcomes of cellular uptake. Data were stated as means ± SEM (n = 3). *P < 0.05, **P < 0.01, ***P < 0.001, compared with control group.

were not heavily involved in the entry of RVG-clocking Zein NPs into U87 cell line. A preferred endocytosis pathway for the Cy5/RVG-Zein to U87 cells may have been clathrin-mediated endocytosis since the NP cellular uptake decreased dramatically with chlorpromazine, from 98.14% to 48.42%. Inhibitors of nAChRs that were effective included benzetimide chloride and PNU-120596. PNU-120596 and Benzethonium chloride considerably reduced the internalization of Cy5/RVG-Zein by the U87 cell line, from 97.97% to 85.78% and 69.15%, respectively. This suggests that the RVG-clocking Zein NPs penetrated the cell membrane by nAChR-mediated

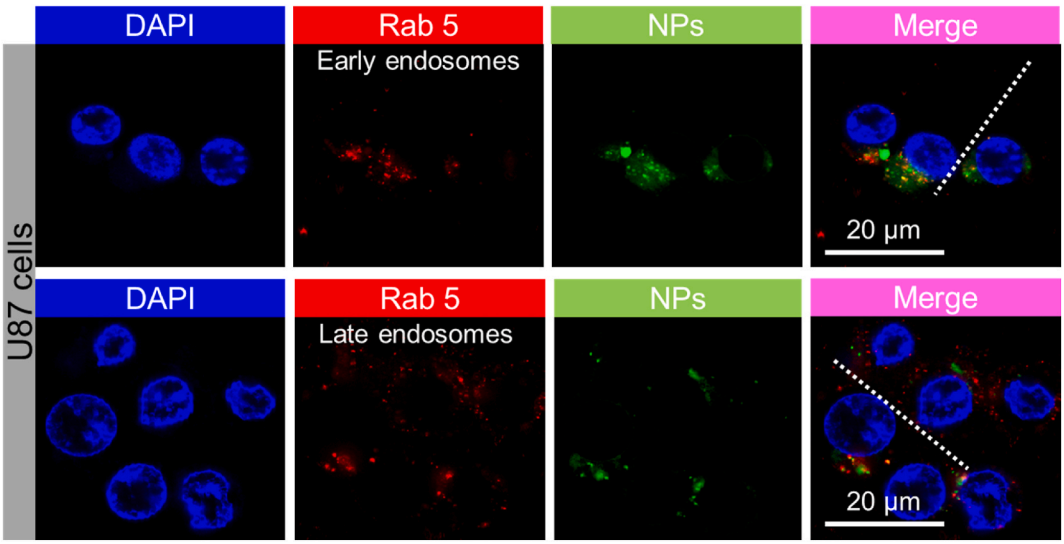

Fig. 7. The cellular internalization of Cy5/TMZ@RVG-Zein NPs in U87 cells. CLSM images of Cy5/TMZ@RVG-Zein (red, NPs) and U87 cells stained with Rab5 (upper), representing early endosomes, and Rab7, demonstrating late endosomes (lower). The scale bar is 20 μm. (For interpretation of the references to colour in this figure legend, the reader is referred to the Web version of this article.)

endocytosis (Fig. 6I).

Rab5 and Rab7, indicators of early and late endosomes, respectively, were used to investigate NP internalization in the U87 cell line (Fig. 7). In endocytosis, NPs would be transferred to endosomes before continuing to organelles. In Fig. 7, the red and green fluorescence lines overlap depicted in the cell region. This suggested that Cy5/TMZ@RVG-Zein colocalized with the early endosomes, as shown in Fig. 7. While Cy5/TMZ@RVG-Zein did not typically colocalize with the late endosomes (Fig. 7), there was significantly fewer overlap of the red and green fluorescence in the cell region in Fig. 7. This data proved that Cy5/TMZ@RVG-Zein NPs could efficiently evade late endosomes during intracellular trafficking and may have been implicated in early endosomes.

We evaluated and studied the cytotoxicity of TMZ, RVG-Zein NPs, and TMZ@RVG-Zein NPs in vitro. Fig. 8A displays the outcomes of treating U87 cell lines with varying doses of TMZ@RVG-Zein NPs, RVG-Zein NP, and pure TMZ. Even at the 10 nM minimal concentration, TMZ effectively inhibited the proliferation of the U87 cell line, as only 49.4% survived treatment. At 10, 25, and 50 nM, TMZ-similar concentrations, there was no discernible difference in cell viability between TMZ and TMZ@RVG-Zein NPs, indicating that both substances were cytotoxic to the U87 cell line. It was demonstrated that the carrier lacked cytotoxicity to the U87 cell line because the cell survival rate was approximately 100% when cultured with different concentrations of the RVG-Zein NPs.

As a marker of programmed cell death, caspase-3 was used in the immunofluorescence analysis [43]. The outcomes can be observed in Fig. 8B, and the cell nuclei were dyed with DAPI, which exhibited blue fluorescence, and caspase-3, which showed green fluorescence. A notable decrease in the quantity of U87 cell line was noted following the administration of TMZ@RVG-Zein NPs at 0.1 and 0.2 μM concentrations, respectively. A colocalization investigation revealed that the U87 cell line contained caspase-3, which fluoresced green, and that blue fluorescence aided the localization of cell nuclei. The control sample without TMZ@RVG-Zein NPs had the highest ratio of caspase-3 +Ve cells, according to 0, 0.1, and 0.2 μM of TMZ@RVG-Zein. The ratio of caspase-3 +Ve cells decreased as the quantity of TMZ@RVG-Zein NPs increased, suggesting that TMZ@RVG-Zein NPs caused cell death by caspase-mediated apoptosis. The nuclei displayed more intense fluorescence following cell treatment with 0.1 and 0.2 μM concentrations of TMZ@RVG-Zein compared to the control sample (Fig. 8C). This suggests that nuclear chromatin and fragmentation are highly prevalent. It was also noted that the U87 cells' morphology changed following treatment with TMZ@RVG-Zein NPs. Findings showed that TMZ@RVG-Zein NPs caused U87 cell lines to undergo caspase-3-mediated cell death.

Further, we examined the U87 cells co-staining with Calcein-AM and PI, which confirmed liver and dead cells (Fig. 9A). TMZ@RVG-Zein NPs, RVG-Zein NP, and pure TMZ were treated with 10 nM minimal concentration to U87 cells for 24 h. The results of the MTT assay and flow cytometry corroborated the observation in Fig. 9A that the combination of TMZ@RVG-Zein NPs could enhance the efficacy of tumour therapy since the control group emitted a uniform green colour, indicating live cells. In contrast, the treatment group displayed red, indicating dead cells. This co-staining method reveals that TMZ@RVG-Zein NPs kill more U87 cells at minimal concentration (Fig. 9B). Fig. 9C shows the results of indicating the U87 cell lines with annexin V-FITC to compare the apoptosis-promoting capabilities of TMZ, TMZ@Zein NPs, and TMZ@RVG. In Fig. 9D, the gating technique was displayed. Comparing the

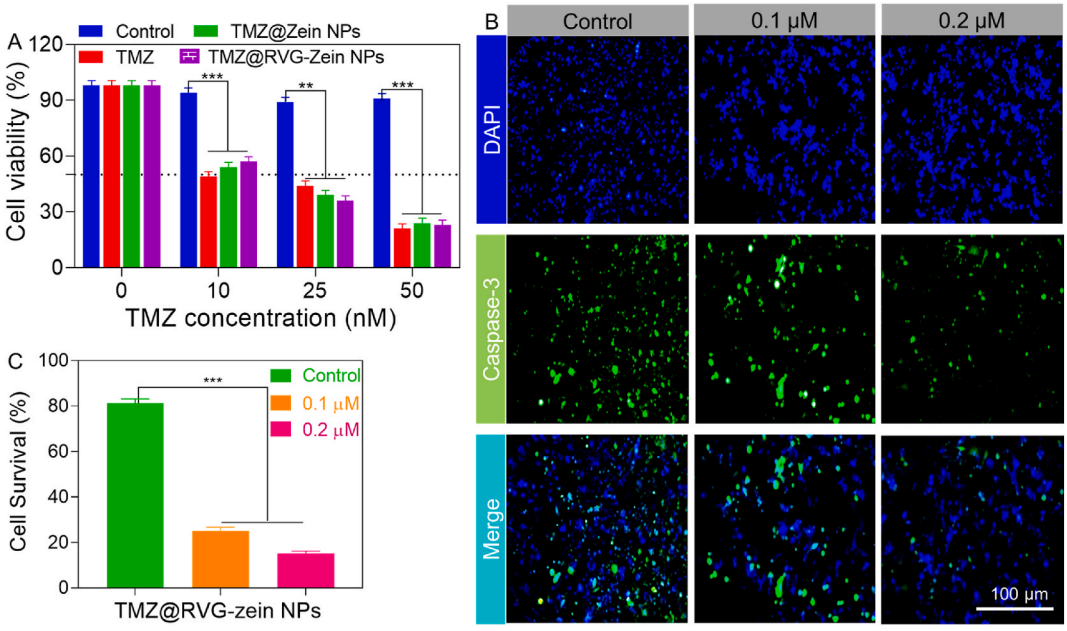

Fig. 8. The in vitro cell viability and caspase-3 image of U87 cells. A) U87 cells treated with TMZ, RVG-Zein NPs, and TMZ@RVG-Zein NPs for 24 h. B) U87 cell lines treated with 0, 0.1, and 0.2 μM of TMZ@RVG-Zein NPs for 24 h. DAPI (blue) stained the cell nuclei, and the cas-3 displayed green fluorescent. The scale bar is 100 μm. C) The apoptotic percentage of U87 cell lines treated with 0.1 and 0.2 μM of TMZ@RVG-Zein NPs attained from Fig. 8A. Data were stated as means ± SEM (n = 3). **P < 0.01, ***P < 0.001, compared with control group. (For interpretation of the references to colour in this figure legend, the reader is referred to the Web version of this article.)

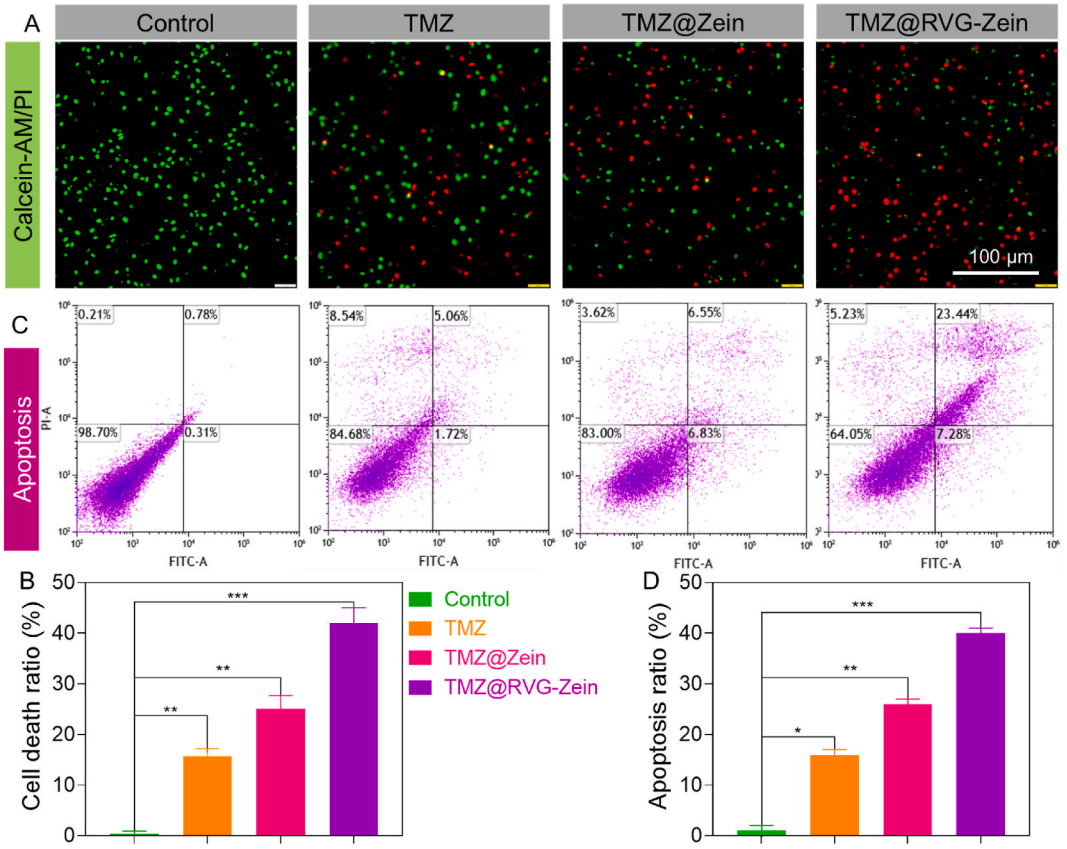

Fig. 9. Live/Dead double staining and Annexin V-FITC double staining. A) U87 cells treated with TMZ, RVG-Zein NPs, and TMZ@RVG-Zein NPs for 24 h for live/dead double staining. The scale bar is 100 μm. B) The bar diagram represents the cell death ratio of the samples. C) U87 cells treated with TMZ, RVG-Zein NPs, and TMZ@RVG-Zein NPs for 24 h for annexin V-FITC double staining. D) The bar diagram represents the apoptosis ratio of the samples. Data were stated as means ± SEM (n = 3). *P < 0.05, **P < 0.01, ***P < 0.001, compared with control group.

apoptotic efficacy of TMZ@RVG-Zein NPs to that of TMZ@Zein NPs and pure TMZ produced similar results respectively.

A bEnd.3 cells monolayer as an in vitro BBB model allowed for further exploration of the RVG-mediated transcytosis of NPs via BBB. Fig. 10A shows the inoculation of the compact cell monolayer on the transwell insert. Three different samples were introduced to the insert and left to incubate for 4 h: Cy5/TMZ, Cy5/TMZ@Zein, and Cy5/TMZ@RVG-Zein. Fig. 10B displayed that the BBB monolayer's transendothelial electrical resistance (TEER) remained relatively unchanged following incubation. Treatments with Cy5/TMZ, Cy5/TMZ@Zein, and Cy5/TMZ@RVG-Zein did not degrade or affect the integrity of the BBB monolayer cells, according to the results. The fluorescence of the transwell's bottom chamber and insert well are shown in Fig. 10B, respectively. Fluorescence from the insert well following a PBS wash revealed that the NPs had been uptake by bEnd.3 cells, as evidenced by their fluorescence. Although the bottom chamber's fluorescence was caused by the NPs there, it had passed through the bEnd.3 monolayer. Cy5/TMZ could not cross the in vitro BBB because it did not glow in the bottom chamber. bEnd.3 cell monolayer and bottom chamber fluorescence were observed in Cy5/TMZ@Zein groups. Zein's capacity to penetrate cell membranes suggests it may help transport the NPs across the cell monolayer of bEnd.3. The Cy5/TMZ@RVG-Zein group showed a much more significant (~2-fold) fluorescence intensity in the bottom chamber and bEnd.3 monolayer compared to the Cy5/TMZ@Zein groups. The results showed that RVG and Zein in TMZ@RVG-Zein helped the compound pass through the blood-brain barrier, although RVG29 was more successful.

5. Conclusions

Here, we effectively developed a new way to deliver drugs to the brain by encapsulating TMZ and RVG29 on the surface of Zein NPs in a self-assembled manner. The result was TMZ@RVG-Zein NPs. In addition to confirming that TMZ was encapsulated in the TMZ@RVG-Zein NPs, the FTIR data also showed that Zein and RVG29 were successfully conjugated. Investigation on TMZ's cytotoxicity in vitro showed that, during the 10–50 nM TMZ comparable concentration range, TMZ@RVG-Zein NPs were equally cytotoxic to U87 cells as pure TMZ. Even though Zein and RVG29 improved NP absorption by U87 cells, RVG29 was more effective. Lastly, the RVG29-clocking Zein NPs show great promise in delivering drugs to the brain to treat diseases affecting the glioblastoma.

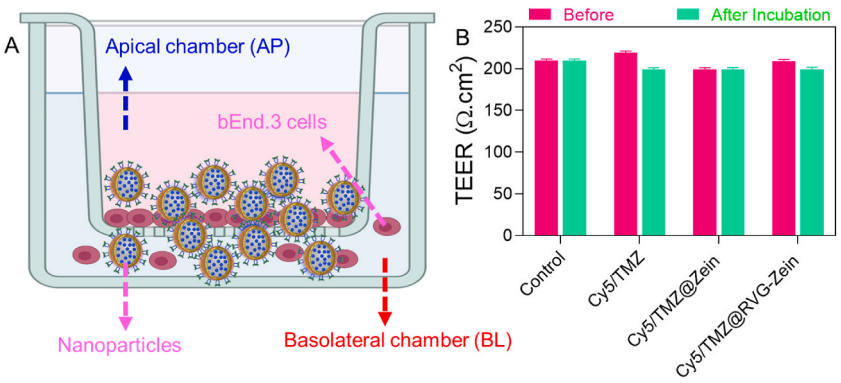

Fig. 10. In vitro blood-brain barrier model and TEER. A) Typical diagram of in vitro BBB. B) The TEER of the BBB cell monolayer was verified after and before the culture with Cy5/TMZ, Cy5/TMZ@Zein, and Cy5/TMZ@RVG-Zein NPs for 4 h.

Ethics declarations

Not applicable.

CRediT authorship contribution statement

Huaming Chen: Writing – original draft, Software, Formal analysis, Data curation, Conceptualization. **Yunhong Wang:** Writing – original draft, Software, Formal analysis, Data curation, Conceptualization. **Hai Wang:** Visualization, Resources, Methodology, Data curation. **Kun Zhang:** Software, Resources, Formal analysis, Data curation. **Yunfei Liu:** Visualization, Validation, Resources, Formal analysis, Data curation. **Qiangfeng Li:** Software, Resources, Methodology. **Chengli Li:** Validation, Software, Methodology, Formal analysis. **Zhonghui Wen:** Writing – review & editing, Writing – original draft, Validation, Supervision, Conceptualization. **Ziyu Chen:** Writing – review & editing, Writing – original draft, Project administration, Conceptualization.

Declaration of competing interest

The authors declare that they have no known competing financial interests or personal relationships that could have appeared to influence the work reported in this paper.

Acknowledgment

Not applicable.

References

[1] A.C. Tan, D.M. Ashley, G.Y. López, M. Malinzak, H.S. Friedman, M. Khasraw, Management of glioblastoma: State of the art and future directions, CA, Cancer J. Clin. 70 (2020) 299–312.
[2] A. Bikfalvi, C.A. da Costa, T. Avril, J.-V. Barnier, L. Bauchet, L. Brisson, P.F. Cartron, H. Castel, E. Chevet, H. Chneiweiss, Challenges in glioblastoma research: focus on the tumor microenvironment, Trends Cancer 9 (2023) 9–27.
[3] M.T. Luiz, L.D. Di Filippo, L.B. Tofani, J.T.C. de Araújo, J.A.P. Dutra, J.M. Marchetti, M. Chorilli, Highlights in targeted nanoparticles as a delivery strategy for glioma treatment, Int. J. Pharm. 604 (2021) 120758.
[4] L. Gallego, V. Ceña, Nanoparticle-mediated therapeutic compounds delivery to glioblastoma, Expet Opin. Drug Deliv. 17 (2020) 1541–1554.
[5] E. Alphandéry, Nano-therapies for glioblastoma treatment, Cancers 12 (2020) 242.
[6] K. Wiwatchaitawee, J.C. Quarterman, S.M. Geary, A.K. Salem, Enhancement of therapies for glioblastoma (GBM) using nanoparticle-based delivery systems, AAPS PharmSciTech 22 (2021) 1–16.
[7] J.-F. Hsu, S.-M. Chu, C.-C. Liao, C.-J. Wang, Y.-S. Wang, M.-Y. Lai, H.-C. Wang, H.-R. Huang, M.-H. Tsai, Nanotechnology and nanocarrier-based drug delivery as the potential therapeutic strategy for glioblastoma multiforme: an update, Cancers 13 (2021) 195.
[8] R. Jnaidi, A.J. Almeida, L.M. Gonçalves, Solid lipid nanoparticles and nanostructured lipid carriers as smart drug delivery systems in the treatment of glioblastoma multiforme, Pharmaceutics 12 (2020) 860.
[9] W. Huang, F. Yao, S. Tian, M. Liu, G. Liu, Y. Jiang, Recent advances in zein-based nanocarriers for precise cancer therapy, Pharmaceutics 15 (2023) 1820.
[10] R. Nunes, A. Baião, D. Monteiro, J. das Neves, B. Sarmento, Zein nanoparticles as low-cost, safe, and effective carriers to improve the oral bioavailability of resveratrol, Drug Deliv. Transl. Res. 10 (2020) 826–837.
[11] A. Raza, U. Hayat, M. Bilal, H.M.N. Iqbal, J.-Y. Wang, Zein-based micro-and nano-constructs and biologically therapeutic cues with multi-functionalities for oral drug delivery systems, J. Drug Deliv. Sci. Technol. 58 (2020) 101818.
[12] X. Yu, H. Wu, H. Hu, Z. Dong, Y. Dang, Q. Qi, Y. Wang, S. Du, Y. Lu, Zein nanoparticles as nontoxic delivery system for maytansine in the treatment of non-small cell lung cancer, Drug Deliv. 27 (2020) 100–109.
[13] L. Zha, B. Wang, J. Qian, B. Fletcher, C. Zhang, Q. Dong, W. Chen, L. Hong, Preparation, characterization and preliminary pharmacokinetic study of pH-sensitive Hydroxyapatite/Zein nano-drug delivery system for doxorubicin hydrochloride, J. Pharm. Pharmacol. 72 (2020) 496–506.
[14] J. Pena-Bahamonde, G. Herrera, S. Lupini, H. Arabaghian, D.F. Rodrigues, Zein nanoparticles for controlled intestinal drug release for the treatment of gastrointestinal infections, ACS Appl. Nano Mater. 6 (2023) 21707–21720.

[15] M.I. Sajid, M. Moazzam, R. Stueber, S.E. Park, Y. Cho, R.K. Tiwari, Applications of amphipathic and cationic cyclic cell-penetrating peptides: significant therapeutic delivery tool, Peptides 141 (2021) 170542.
[16] S. Huang, Z. Zhu, B. Jia, W. Zhang, J. Song, Design of acid-activated cell-penetrating peptides with nuclear localization capacity for anticancer drug delivery, J. Pept. Sci. 27 (2021) e3354.
[17] S. Khan, Y. Vahdani, A. Hussain, S. Haghighat, F. Heidari, M. Nouri, S.H. Bloukh, Z. Edis, M.M.N. Babadaei, M. Ale-Ebrahim, Polymeric micelles functionalized with cell penetrating peptides as potential pH-sensitive platforms in drug delivery for cancer therapy: a review, Arab, J. Chem. 14 (2021) 103264.
[18] Q. Zhang, N. Liu, J. Wang, Y. Liu, K. Wang, J. Zhang, X. Pan, The recent advance of cell-penetrating and tumor-targeting peptides as drug delivery systems based on tumor microenvironment, Mol. Pharm. 20 (2023) 789–809.
[19] J. Song, S. Huang, Z. Zhang, B. Jia, H. Xie, M. Kai, W. Zhang, SPA: a peptide antagonist that acts as a cell-penetrating peptide for drug delivery, Drug Deliv. 27 (2020) 91–99.
[20] C.P. Cerrato, Ü. Langel, An update on cell-penetrating peptides with intracellular organelle targeting, Expet Opin. Drug Deliv. 19 (2022) 133–146.
[21] A. Shoari, R. Tooyserkani, M. Tahmasebi, D.W.P.M. Löwik, Delivery of various cargos into cancer cells and tissues via cell-penetrating peptides: a review of the last decade, Pharmaceutics 13 (2021) 1391.
[22] S. Reissmann, M.P. Filatova, New generation of cell-penetrating peptides: functionality and potential clinical application, J. Pept. Sci. 27 (2021) e3300.
[23] L. Gomes dos Reis, D. Traini, Advances in the use of cell penetrating peptides for respiratory drug delivery, Expet Opin. Drug Deliv. 17 (2020) 647–664.
[24] M. Ren, Y. Zhou, T. Tu, D. Jiang, M. Pang, Y. Li, Y. Luo, X. Yao, Z. Yang, Y. Wang, RVG peptide-functionalized favipiravir nanoparticle delivery system facilitates antiviral therapy of neurotropic virus infection in a mouse model, Int. J. Mol. Sci. 24 (2023) 5851.
[25] R. Zhou, L. Zhu, Z. Zeng, R. Luo, J. Zhang, R. Guo, L. Zhang, Q. Zhang, W. Bi, Targeted brain delivery of RVG29-modified rifampicin-loaded nanoparticles for Alzheimer's disease treatment and diagnosis, Bioeng. Transl. Med. 7 (2022) e10395.
[26] Y.-C. Kuo, Y.-J. Lee, R. Rajesh, Enhanced activity of AZD5582 and SM-164 in rabies virus glycoprotein-lactoferrin-liposomes to downregulate inhibitors of apoptosis proteins in glioblastoma, Biomater. Adv. 133 (2022) 112615.
[27] Q. Wang, S. Cheng, F. Qin, A. Fu, C. Fu, Application progress of RVG peptides to facilitate the delivery of therapeutic agents into the central nervous system, RSC Adv. 11 (2021) 8505–8515.
[28] F. Ji, L. Xu, K. Long, F. Zhang, M. Zhang, X. Lu, M. Xia, J. Chen, Y. Du, Y. Tang, Rabies virus glycoprotein 29 (RVG29) promotes CAR-T immunotherapy for glioma, Transl. Res. (2023).
[29] E.P. Chung, J.D. Cotter, A. V Prakapenka, R.L. Cook, D.M. DiPerna, R.W. Sirianni, Targeting small molecule delivery to the brain and spinal cord via intranasal administration of rabies virus glycoprotein (RVG29)-modified PLGA nanoparticles, Pharmaceutics 12 (2020) 93.
[30] R. Wang, Q. Liang, X. Zhang, Z. Di, X. Wang, L. Di, Tumor-derived exosomes reversing TMZ resistance by synergistic drug delivery for glioma-targeting treatment, Colloids Surf. B Biointerfaces 215 (2022) 112505.
[31] A. Khosa, K. V Krishna, S.K. Dubey, R.N. Saha, Lipid nanocarriers for enhanced delivery of temozolomide to the brain, Drug Deliv. Syst. (2020) 285–298.
[32] R.R. Kudarha, K.K. Sawant, Hyaluronic acid conjugated albumin nanoparticles for efficient receptor mediated brain targeted delivery of temozolomide, J. Drug Deliv. Sci. Technol. 61 (2021) 102129.
[33] L.D. Di Filippo, J.H. Azambuja, J.A.P. Dutra, M.T. Luiz, J.L. Duarte, L.R. Nicoleti, S.T.O. Saad, M. Chorilli, Improving temozolomide biopharmaceutical properties in glioblastoma multiforme (GBM) treatment using GBM-targeting nanocarriers, Eur. J. Pharm. Biopharm. 168 (2021) 76–89.
[34] Z. Song, X. Huang, J. Wang, F. Cai, P. Zhao, F. Yan, Targeted delivery of liposomal temozolomide enhanced anti-glioblastoma efficacy through ultrasound-mediated blood–brain barrier opening, Pharmaceutics 13 (2021) 1270.
[35] P.S. Yasaswi, K. Shetty, K.S. Yadav, Temozolomide nano enabled medicine: promises made by the nanocarriers in glioblastoma therapy, J. Contr. Release 336 (2021) 549–571.
[36] Z. Li, Y. Yang, H. Wei, X. Shan, X. Wang, M. Ou, Q. Liu, N. Gao, H. Chen, L. Mei, X. Zeng, Charge-reversal biodegradable MSNs for tumor synergetic chemo/photothermal and visualized therapy, J. Contr. Release 338 (2021) 719–730, https://doi.org/10.1016/j.jconrel.2021.09.005.
[37] N. Gupta, D. Santhiya, A. Aditya, Tailored smart bioactive glass nanoassembly for dual antibiotic in vitro sustained release against osteomyelitis, J. Mater. Chem. B 4 (2016) 7605–7619, https://doi.org/10.1039/C6TB01528J.
[38] W. Zheng, H. Song, Z. Luo, H. Wu, L. Chen, Y. Wang, H. Cui, Y. Zhang, B. Wang, W. Li, Acetylcholine ameliorates colitis by promoting IL-10 secretion of monocytic myeloid-derived suppressor cells through the nAChR/ERK pathway, Proc. Natl. Acad. Sci. USA 118 (2021) e2017762118.
[39] M. Hameed, S. Panicker, S.H. Abdallah, A.A. Khan, C. Han, M.M. Chehimi, A.A. Mohamed, Protein-coated aryl modified gold nanoparticles for cellular uptake study by osteosarcoma cancer cells, Langmuir 36 (2020) 11765–11775, https://doi.org/10.1021/acs.langmuir.0c01443.
[40] R. Zhang, X. Qin, F. Kong, P. Chen, G. Pan, Improving cellular uptake of therapeutic entities through interaction with components of cell membrane, Drug Deliv. 26 (2019) 328–342.
[41] B. He, D. Yang, M. Qin, Y. Zhang, B. He, W. Dai, X. Wang, Q. Zhang, H. Zhang, C. Yin, Increased cellular uptake of peptide-modified PEGylated gold nanoparticles, Biochem. Biophys. Res. Commun. 494 (2017) 339–345.
[42] J.-R. Liang, H. Yang, Ginkgolic acid (GA) suppresses gastric cancer growth by inducing apoptosis and suppressing STAT3/JAK2 signaling regulated by ROS, Biomed. Pharmacother. 125 (2020) 109585, https://doi.org/10.1016/j.biopha.2019.109585.
[43] N.U. Khaliq, D.Y. Park, H.J. Lee, K.S. Oh, J.H. Seo, S.Y. Kim, C.S. Hwang, T.-H. Lim, S.H. Yuk, Pluronic/heparin nanoparticles for chemo-photodynamic combination cancer therapy through photoinduced caspase-3 activation, ACS Appl. Nano Mater. 1 (2018) 2943–2952, https://doi.org/10.1021/acsanm.8b00572.